UCRL-TR-225197

LAWRENCE
LIVERMORE
NATIONAL
LABORATORY

Source tilting within the difference formulation for radiation transport

T. Luu, E. Brooks, A. Szoke

October 10, 2006

This document was prepared as an account of work sponsored by an agency of the United States Government. Neither the United States Government nor the University of California nor any of their employees, makes any warranty, express or implied, or assumes any legal liability or responsibility for the accuracy, completeness, or usefulness of any information, apparatus, product, or process disclosed, or represents that its use would not infringe privately owned rights. Reference herein to any specific commercial product, process, or service by trade name, trademark, manufacturer, or otherwise, does not necessarily constitute or imply its endorsement, recommendation, or favoring by the United States Government or the University of California. The views and opinions of authors expressed herein do not necessarily state or reflect those of the United States Government or the University of California, and shall not be used for advertising or product endorsement purposes.

This work was performed under the auspices of the U.S. Department of Energy by University of California, Lawrence Livermore National Laboratory under Contract W-7405-Eng-48.

Source tilting within the difference formulation for radiation transport ⋆

Thomas Luu *, Eugene D. Brooks III, Abraham Szőke

University of California, Lawrence Livermore National Laboratory, P.O. Box 808, Livermore, CA 94550, USA

Abstract

We apply a heuristic technique known as "source tilting" to a Monte Carlo solution for radiation transport, in the difference formulation, that otherwise employs a piecewise-constant treatment of the material temperature. Source tilting improves the accuracy of the piecewise-constant treatment, reducing the excessive energy flow that occurs in the thick limit. An analysis of the cause of excessive energy flow suggests an interpolation scheme that removes this defect, obtaining the correct diffusion limit flux between zones. The results obtained with our interpolation scheme agree almost identically to those of a self-consistent piecewise-linear treatment of the difference formulation while avoiding its additional costs. The resulting method is capable of providing robust and accurate calculations for problems involving optically thick zones. We comment on the monotonicity issues that arise when employing this transport method.
UCRL-JRNL-225197

Key words: difference formulation, radiation transport, implicit Monte Carlo, source tilting

1 Introduction

In computational radiation transport, there has been a substantial amount of recent interest in algorithms that have the diffusion limit [1]. These algorithms are more generally referred to as asymptotic-preserving discretization schemes

⋆ This work was performed under the auspices of the U.S. Department of Energy by the University of California, Lawrence Livermore National Laboratory under contract No. W-7405-Eng-48.
* Corresponding Author:
Email address: luu5@llnl.gov (Thomas Luu).

[2]. A discretization of the transport equation is said to have the diffusion limit, or be asymptotic-preserving, if it provides a valid discretization of the diffusion equation obtained from the transport equation using a continuum asymptotic analysis, when a similar asymptotic analysis is applied to the discretization of the transport equation. If the discretization of the transport equation is asymptotic-preserving in this sense it will provide accurate solutions as the physical system approaches the diffusion limit, without having to shrink the zone sizes, or time steps, to scales that are small compared to the mean free path, or mean free time, of a photon.

The development of asymptotic-preserving transport algorithms has progressed for both deterministic and Monte Carlo solution methods. Beyond the relevant work referred to in [1], significant progress was made in this area for the S_n method applied to the non-linear transport of thermally emitted photons [3]. More recently, the Monte Carlo treatment of the transport equation has been extended to a self-consistent piecewise-linear treatment of the material state variable, first for a linearized grey treatment in the standard formulation of radiative transport [4], then in the difference formulation [5]. The result is a robust treatment that is accurate in the presence of optically thick zones, as was the case for the earlier work employing the S_n method.

The Implicit Monte Carlo (IMC) algorithm [6], augmented by random walk and source tilting [7], has been an effective tool for the transport of thermally emitted photons for quite some time. The random walk process softens the deleterious computational impact of effective scattering, while source tilting is used to reduce the teleportation of thermal energy caused by the piecewise-constant treatment of the material temperature as the time step size is reduced. Although IMC has been a workhorse for some time it does not provide correct coupling between the radiation field and the material energy [8,9].

The difference formulation for the transport of thermally emitted photons [10] removes the issue of computational efficiency associated with a Monte Carlo treatment of photon transport in a thick system. A self-consistent piecewise-linear treatment of the material state variable in the difference formulation removes the energy teleportation problem associated with the energy absorbed on one side of a zone immediately causing emission of thermal energy on the other side of the zone. Although the implementation of a self-consistent piecewise-linear treatment of the difference formulation in higher dimensions is possible in principle, the task of implementing all of the required particle types and associated scoring arrays is daunting.

With due respect for the self-consistent piecewise-linear treatments for the transport of thermally emitted photons, the question of whether or not a variation on the theme of source tilting [7] can successfully address the issue of energy teleportation, while avoiding the higher cost of a self-consistent

piecewise-linear treatment, is still open. This question is especially important when considering integrating the difference formulation with hydrodynamics codes that otherwise implement the material state variables as constant functions of space within a zone.

Fleck and Canfield [7] argue that the spatial sampling of Monte Carlo source particles in optically thick media must be consistent with the spatial gradients of the material state variable, $\Phi = aT^4$, if transport in such media is to be calculated accurately. In their paper, they consider a linear (within a zone) spatial sampling scheme, with the slope derived from the values of Φ in nearest neighbor zones. This sampling scheme has become known as "source tilting," or just "tilting," in the lore of the IMC algorithm, because the constant value of Φ in a zone is tilted in order to produce the spatial distribution of source particles. More formally, in this scheme the piecewise-constant form for $\Phi(x)$ in the problem domain is mapped onto a piecewise-linear function in some prescribed fashion.

In this paper we investigate two such mappings in the context of the difference formulation. The first, which we call "source tilting," is identical to the scheme of Fleck and Canfield. The details of this scheme in the difference formulation, and an analysis of its consequences, are described in Sect. 4. It is in this analysis that the goal of source tilting is more clearly understood, this being that of getting the flux (between zones) produced by the Monte Carlo simulation to agree with the correct continuum diffusion limit, and as a result produce an asymptotic-preserving algorithm. It is the discontinuity in the value of Φ at a zone boundary, when it is not physical, that produces excessive flux between adjoining zones.

The results of the analysis of source tilting inspires a second "interpolation" scheme. Recognizing that unphysical discontinuities in $\Phi(x)$ are the source of excess flux between zones in the optically thick limit, we remove these discontinuities by using linear interpolation of Φ between zone centers. This produces the correct diffusion limit for the flux between zones. Zone interfaces where sharp discontinuities in the material opacity occur are dealt with by carefully handling the derivative of $\Phi(x)$ approaching the discontinuity from the left, and the right. This interpolation scheme, described in Sect. 5, provides solutions nearly identical to those of a self-consistent piecewise-linear finite element method and is our preferred method for practical calculations.

In Sect. 2 we give a cursory review of the difference formulation. Section 3 describes the piecewise-constant implementation of the difference formulation, supporting a segue to Sects. 4 and 5 that explain our source tilting and interpolation algorithms, respectively. We show computational results in Sect. 6, comparing them with those of piecewise-constant and self-consistent piecewise-linear calculations. We also compare our results with those of recently pub-

lished benchmark calculations. We perform a computational error analysis of our algorithms and comment on monotonicity issues, giving physical arguments and constraints for when monotonicity is not violated. Section 9 recaps our results and contains our conclusions. To keep the presentation concise, we reserve lengthy derivations for appendices.

2 Difference formulation

Radiation transport in media is described by the Boltzmann equation for photons coupled to the material energy equation,

$$\frac{1}{c}\frac{\partial I}{\partial t} + \Omega \cdot \nabla I = -\sigma_a (I - B) \quad , \tag{1}$$

$$\frac{\partial E_{mat}}{\partial t} = \int d\nu \int d\Omega \sigma_a (I - B) + G \quad , \tag{2}$$

respectively. Here I represents the intensity field, σ_a the absorption cross section, $B = \frac{2h\nu^3}{c^2}(e^{h\nu/kT} - 1)^{-1}$ is the blackbody field, E_{mat} the energy of the material, ν the frequency, G is a volumetric heat source, and Ω the direction of travel for photons. It is assumed that the material is in local thermal equilibrium (LTE) at the material temperature, T. In this formulation for radiative transport, we assume that there is no physical scattering and that the medium is static. The difference formulation for photon transport,

$$\frac{1}{c}\frac{\partial D}{\partial t} + \Omega \cdot \nabla D = -\sigma_a D - \frac{1}{c}\frac{\partial B}{\partial t} - \Omega \cdot \nabla B \quad , \tag{3}$$

$$\frac{\partial E_{mat}}{\partial t} = \int d\nu \int d\Omega \sigma_a D + G \quad , \tag{4}$$

is obtained from the standard formulation, Eqs. (1) and (2) above, by defining the photon intensity field relative to a Planckian at the local material temperature, using the definition $D = I - B$. The two formulations for the transport of thermally emitted photons are formally equivalent. The benefit of working with the difference formulation, at least when employing a Monte Carlo solution technique, is that noise is greatly reduced in the thick limit [11].

Although the derivative nature of the source terms in the difference formulation,

$$-\frac{1}{c}\frac{\partial B}{\partial t} - \Omega \cdot \nabla B \quad , \tag{5}$$

appears complicated, these sources are relatively easy to implement in a Monte Carlo solution of the transport equation. The fact that the sources are indepen-

dent of the material opacity allows them to be sampled without uncontrolled approximations, leading to a cleaner and more efficient implementation, compared to the standard formulation of transport. The frequency dependence of the source terms is factored out using the chain rule,

$$-\frac{1}{c}\frac{\partial B}{\partial t} - \mu\frac{\partial B}{\partial x} = \frac{4\pi}{c}\frac{\partial B}{\partial \Phi}\left[-\frac{1}{4\pi}\frac{\partial \Phi(x,t)}{\partial t} - \frac{\mu c}{4\pi}\frac{\partial \Phi(x,t)}{\partial x}\right] \quad , \tag{6}$$

and it can be shown that $(4\pi/c)\partial B/\partial\Phi$ is a frequency distribution, since is it is positive and its frequency integral is unity [10,5]. Here $\Phi = aT^4$ is the radiation energy density of a black body at the material temperature. We have assumed slab geometry and μ is the cosine of the direction of the radiation relative to the x-axis. For the remainder of the paper we will present results in slab geometry.

3 Piecewise-constant implementation

The basic discretization strategy used in this paper is identical to the one used in [11]. The problem is divided into N zones, enumerated by $i \in (1, N)$. The position of the left edge of zone i is x_i. The position of its right edge is x_{i+1}, this also being the position of the left edge of the next zone. The value of the material state variable, T, or equivalently $\Phi = aT^4$, is a constant function of space within each zone as depicted by the shaded regions of Fig. B.1. Its values are denoted as Φ_i. The material energy density, E_{mat}, and the material opacity, σ_a, are treated as constant functions of space within each zone as well. These material properties may be represented by simple formulas, or by more complicated physical data tables indexed by the material temperature and density, as the case may be. If the boundary conditions for a problem are defined as thermal baths, the boundary condition for the left side is Φ_0 and the boundary condition for the right side is Φ_{N+1}.

The temporal treatment of the material state variable, Φ, is piecewise-constant in time. However, it is treated implicitly (as in backward-Euler), taking on its unknown end of time step value immediately after the beginning of the time step, t_0, for the duration of the time step, Δt. This is done in order to obtain unconditional stability for the time evolution of a problem. If the opacity of the material is a function of the material state variable it is evaluated using the known value of the material state variable at the beginning of the time step. In order to be able to run the Monte Carlo solution of the transport equation, the frequency distribution of source particles $(4\pi/c)\partial B/\partial\Phi$ is also evaluated explicitly, using the known value of the material state variable at the beginning of the time step. The details of sampling the frequency distribution of the source terms are included in [10,5].

The gradient source term is zero within each zone i since the field Φ_i is constant there. Because of the discontinuities at zone interfaces, the gradient source terms are

$$-\frac{\mu c}{4\pi}\frac{\partial \Phi}{\partial x} = -\frac{\mu c}{4\pi}\sum_{i=1}^{N+1}\delta(x-x_i)\left(\Phi_i(t_0+\Delta t)-\Phi_{i-1}(t_0+\Delta t)\right) \quad . \tag{7}$$

Here $\delta(x-x_i)$ is the Dirac delta function and the $\Phi_i(t_0+\Delta t)$ are unknown values of the material state variable that must be implicitly solved for. Note that there are $N+1$ zone interfaces.

To determine the sources due to the time derivative term in Eq. (6), we assume that the fields immediately jump to their end of time step values at the beginning of the time step. This gives

$$-\frac{1}{4\pi}\frac{\partial \Phi_i}{\partial t} = -\frac{1}{4\pi}\delta(t-t_0)[\Phi_i(t_0+\Delta t)-\Phi_i(t_0)] \quad . \tag{8}$$

This source is constant as a function of space within each zone and thus sampled uniformly with a partially unknown factor $[\Phi_i(t_0+\Delta t)-\Phi_i(t_0)]$.

The implementation of the angular and spatial distribution of the source terms is obtained by writing them in terms of distribution functions for the generalized particle coordinates. For a thorough discussion of this, the reader is referred to [10] and references within.

The unknowns, $\Phi_i(t_0+\Delta t)$, are calculated by solving the energy balance equation, Eq. (4), at the end of the time step, $t_0+\Delta t$. To accomplish this, we first formally integrate Eq. (4) from t_0 to $t_0+\Delta t$ to obtain the following function,

$$\begin{aligned} f(x) &= E_{mat}(T(x,t_0)) - E_{mat}(T(x,t_0+\Delta t)) \\ &+ 2\pi\int_{t_0}^{t_0+\Delta t} dt \int d\nu \int d\mu \sigma_a(\nu, T(x,t_0)) D(x,t;\nu,\mu) + \int_{t_0}^{t_0+\Delta t} dt\ G(x,t) \quad . \end{aligned} \tag{9}$$

We then integrate $f(x)$ within each zone, thereby defining the following quantities,

$$\begin{aligned} f_j &= \int_{x_j}^{x_{j+1}} dx f(x) \quad , \\ &= E_j(t_0) - E_j(t_0+\Delta t) + (\sigma D)_j + G_j \quad , \end{aligned} \tag{10}$$

where

$$E_j = \int_{x_j}^{x_{j+1}} dx E_{mat}(T) = \Delta x_i \frac{\rho c_\nu}{a^{1/4}} \ \Phi_i^{1/4} \quad , \tag{11}$$

$$G_j = \int_{x_j}^{x_{j+1}} dx G(x,T) \quad , \tag{12}$$

and

$$\begin{aligned}(\sigma D)_j &= 2\pi \int_{x_j}^{x_{j+1}} dx \int_{t_0}^{t_0+\Delta t} dt \int d\nu \int d\mu \sigma_a(\nu, T(x,t_0)) D(x,t;\nu,\mu) \\ &= N_j \\ &+ \sum_i (DDT)_j^i \ (\Phi_i(t_0) - \Phi_i(t_0+\Delta t)) \\ &+ \sum_i (DDX)_j^i \ (\Phi_{i-1}(t_0+\Delta t) - \Phi_i(t_0+\Delta t)) \quad .\end{aligned} \tag{13}$$

We have assumed that ρc_ν is constant within each zone, during the time step, and N_j is the contribution from the census particles to zone j from the prior time step, $(DDT)_j^i$ is the contribution to zone j from the time-derivative sources emanating from zone i, and $(DDX)_j^i$ is the contribution to zone j from delta function sources from zone edge i. Note the non-linearity of Φ in Eq. (11). Our unknown $\Phi_i(t_0+\Delta t)$ are found by demanding that $f_j = 0$ for all j. We solve for these by way of a Newton-Raphson iteration algorithm.

When zone sizes are much greater than one mean free path, the piecewise-constant implementation of the difference formulation suffers from excessive energy flow for both time dependent problems and situations approaching steady state. To gain some understanding of this issue, consider a finite slab of thickness L, composed of a material with a constant absorption coefficient, σ. The material is heated on the left with a thermal bath, Φ_L, and cooled on the right with a thermal bath, Φ_R, with $\Phi_L > \Phi_R$. We consider the situation where steady state has been reached, with a constant flux of energy, F, flowing to the right.

Within the slab, in the continuum diffusion limit [10], the flux is given by

$$F = -\frac{ca}{3\sigma}\frac{\partial T^4}{\partial x} = -\frac{c}{3\sigma}\frac{\partial \Phi}{\partial x} \quad . \tag{14}$$

Since F is constant, Eq. (14) states that Φ is linear as a function of space within the problem volume where the diffusion limit is valid. The diffusion limit is not valid in the boundary layers within one mean free path, or so, of the problem boundaries. For the purpose of this discussion we can ignore the corrections needed to accommodate this detail.

In our piecewise-constant discretization, as the problem approaches steady state, we may ignore the $\partial\Phi/\partial t$ source term. The remaining sources are the

$\partial\Phi/\partial x$ sources due to the discontinuities in Φ that occur at the boundaries between zones. Under conditions that each zone is optically thick, $(x_{i+1} - x_i)\sigma \gg 1$, these sources are completely absorbed in the zone that they are directed into. The flux leaving each zone boundary at x_i traveling to the right is computed by integrating the source for positive μ,

$$F(x_i) = \frac{c}{4}(\Phi_{i-1} - \Phi_i) \quad . \tag{15}$$

An equal amount of negative source leaves the zone boundary in the opposite direction.

When the piecewise-constant discretization of the problem reaches steady state, the flux at all of the interfaces between the zones is the same, and by Eq. (15) the step in the value of Φ at all of the interfaces is the same. The total change in Φ, $\Phi_L - \Phi_R$, is distributed across $N + 1$ interfaces, and the flux traveling across the problem is

$$F = \frac{c}{4}\frac{(\Phi_L - \Phi_R)}{N+1} \quad . \tag{16}$$

It is obvious from Eq. (16) that computational results using a piecewise-constant treatment of the source terms will poorly represent optically thick zones as the flux does not depend upon the opacity as it should. By suitably adjusting the zone sizes, subject to the constraint that zones remain optically thick, any monotonic solution for $\Phi(x)$ can be obtained. Figure B.3 shows examples of how the steady state solution of Φ, obtained from actual Monte Carlo simulations, can change due to the zoning of the problem. Here a steady state profile of $\Phi = aT^4(x)$ is plotted. The changes in zoning are apparent from the figure. In all three cases, the solution is monotonic, but can strongly differ from the correct solution: a straight diagonal line. To obtain an accurate solution properly driven by the physics one must ensure that *all* of the zones in the problem are optically thin.

In order to get the correct flux for a problem with optically thick zones, we must go beyond a piecewise-constant treatment of the material state variable. The symbolic implicit Monte Carlo (SIMC) method, in the difference formulation, was extended to a self-consistent piecewise-linear treatment of the material state variable in [5], following the lead of [4] who did it for a linearized form of the standard formulation of transport. The implementation of the self-consistent piecewise-linear method is complicated, and more expensive, but it produces accurate solutions for optically thick zones. An open question is whether or not source tilting, or a variation on this theme, can obtain these same accuracy benefits at a lower computational cost. In the next sections, we turn to the construction and evaluation of suitable schemes for the difference formulation.

4 Source tilting

In this scheme, reformulating what appears in [7], the tilted value of Φ to use within zone i, $\widetilde{\Phi}_i(x)$, is constructed by matching the slope of the line found by connecting the centers of the neighboring zones. The slope m using this construction is

$$m = 2\left(\frac{\Phi_{i+1} - \Phi_{i-1}}{x_{i+2} - x_i + x_{i+1} - x_{i-1}}\right) \quad . \tag{17}$$

We require that this prescription does not change the total integrated source strength of the original piecewise-constant profile, thus keeping the total energy emitted by the tilted sources the same as their piecewise-constant counterparts. This is done by tilting about the value Φ_i at the center of the zone. By inspection, the following expression for $\widetilde{\Phi}_i(x)$ satisfies this requirement:

$$\widetilde{\Phi}_i(x) = 2\left[\frac{\Phi_{i+1} - \Phi_{i-1}}{x_{i+2} - x_i + x_{i+1} - x_{i-1}}\right](x - \frac{1}{2}(x_{i+1} + x_i)) + \Phi_i \qquad x_i \leq x < x_{i+1} \quad . \tag{18}$$

Defining the basis functions $\chi_i^1(x)$ and $\chi_i^2(x)$ as

$$\chi_i^1(x) = \frac{x_{i+1} - x}{x_{i+1} - x_i} \quad , \tag{19}$$
$$\chi_i^2(x) = \frac{x - x_i}{x_{i+1} - x_i} \quad ,$$

Eq. (18) can be recast as

$$\widetilde{\Phi}_i(x) = \Phi_i^1 \chi_i^1(x) + \Phi_i^2 \chi_i^2(x) \quad , \tag{20}$$

where

$$\Phi_i^1 = (\Phi_{i+1} - \Phi_{i-1})\frac{(x_i - x_{i+1})}{(x_{i+2} - x_i + x_{i+1} - x_{i-1})} + \Phi_i \quad , \tag{21}$$
$$\Phi_i^2 = (\Phi_{i+1} - \Phi_{i-1})\frac{(x_{i+1} - x_i)}{(x_{i+2} - x_i + x_{i+1} - x_{i-1})} + \Phi_i \quad . \tag{22}$$

The basis functions of Eq. (19) allow us to express our tilted field in a compact way.

Equations (18) through (22) are valid for interior zones where the zone in question has nearest neighbor zones on either side. For zones adjoining a problem boundary, the prescription for performing the tilt must be modified. In these cases, the slope is determined by a line connecting the centers of the nearest neighbor zone and the boundary zone. For the left zone boundary, one has

$$\Phi_1^1 = \Phi_1 - (\Phi_2 - \Phi_1)\frac{(x_2 - x_1)}{(x_3 - x_1)} \quad , \tag{23}$$

$$\Phi_1^2 = \Phi_1 + (\Phi_2 - \Phi_1)\frac{(x_2 - x_1)}{(x_3 - x_1)} \quad . \tag{24}$$

The right boundary zone has

$$\Phi_N^1 = \Phi_N - (\Phi_N - \Phi_{N-1})\frac{(x_{N+1} - x_N)}{(x_{N+1} - x_{N-1})} \quad , \tag{25}$$

$$\Phi_N^2 = \Phi_N + (\Phi_N - \Phi_{N-1})\frac{(x_{N+1} - x_N)}{(x_{N+1} - x_{N-1})} \quad . \tag{26}$$

Figure B.1 shows an example of the tilted field when constructed from an original piecewise-constant field. Note that for this tilt prescription, the temperatures on the left- and right-hand side of an interface between zones are usually not equal, leading to a discontinuous $\widetilde{\Phi}(x)$.

The source terms for the tilted treatment of Φ are constructed by making the replacement $\Phi \rightarrow \widetilde{\Phi}$ in the time derivative and gradient terms of Eq. (6). We now examine these source terms in greater detail. There are two contributions to the gradient source: contributions from within a zone due to the fact that $\widetilde{\Phi}_i(x)$ is not constant within zone i, and a residual contribution from the zone edges because Φ_i^2 is not equal to Φ_{i+1}^1, in general. Within zone i, the gradient source term is

$$-\frac{\mu c}{4\pi}\frac{\partial \widetilde{\Phi}_i}{\partial x} = -\frac{\mu c}{4\pi}\frac{\Phi_i^2 - \Phi_i^1}{x_{i+1} - x_i} \quad . \tag{27}$$

Substituting the values for Φ_i^1 and Φ_i^2 obtained from Eqs. (21) and (22), respectively, or the slope directly from Eq. (17), we obtain

$$-\frac{\mu c}{4\pi}\frac{\partial \widetilde{\Phi}_i}{\partial x} = -\frac{\mu c}{2\pi}\frac{\Phi_{i+1} - \Phi_{i-1}}{x_{i+2} - x_i + x_{i+1} - x_{i-1}} \quad . \tag{28}$$

Note that the gradient source term within zone i does not depend upon Φ_i. For zone 1 and zone N, the boundary zones for the problem, the special cases of Eqs. (23) through (26) are used to construct this source term.

At the boundary between zones a singular contribution to the gradient source term occurs due to the discontinuity in $\widetilde{\Phi}$ that appears there:

$$-\frac{\mu c}{4\pi}\delta(x - x_i)(\Phi_{i+1}^1 - \Phi_i^2) \quad . \tag{29}$$

This source term is expanded in terms of the Φ_i by substituting Φ_{i+1}^1 and Φ_i^2, defined in Eq. (19). It is instructive to consider the case where the zone sizes

are equal. The singular contribution to the gradient, at x_i, in this case is

$$-\frac{\mu c}{4\pi}\delta(x-x_i)\left(\frac{3}{4}(\Phi_i-\Phi_{i-1})-\frac{1}{4}(\Phi_{i+1}-\Phi_{i-2})\right) \quad . \tag{30}$$

Comparing Eqs. (30) and (7), it can be seen that the effect of source tilting reduces the source strength at the edges between zones. To the degree that the four (zone center) values, $\{\Phi_{i-2},\ \Phi_{i-1},\ \Phi_i,\ \Phi_{i+1}\}$, fall on a straight line, as a function of x, the strength of the singular contribution to the $\partial\Phi/\partial x$ source term is reduced to zero.

Assuming that $\widetilde{\Phi}(t)$ jumps immediately to the end of time step value at the beginning of the time step, the time-derivative source term gives

$$-\frac{1}{4\pi}\frac{\partial\widetilde{\Phi}_i}{\partial t}=-\frac{1}{4\pi}\delta(t-t_0)\sum_{l=1}^{2}-(\Phi_i^l(t_0+\Delta t)-\Phi_i^l(t_0))\chi_i^l(x) \quad . \tag{31}$$

Except for the fact that we must expand the Φ_i^l in terms of the Φ_i using Eqs. (19) through (22), this source term has the same form as the equivalent one in the self-consistent piecewise-linear treatment [5]. It is sampled in an identical manner. For a detailed analysis of these source terms, the reader is referred to [5] and the references within.

In a piecewise-constant treatment of the material state variable, the source particles due to $\partial\Phi/\partial t$ are emitted uniformly within each zone. However, tilting requires additional source particles to be emitted with a linear distribution (due to x-dependence in Eq. (31)) within each zone. Due to the tilting of sources, the unknown factor in the weight of a photon depends on the three terms $\Phi_{i+1}(t_0+\Delta t)$, $\Phi_{i-1}(t_0+\Delta t)$, and $\Phi_i(t_0+\Delta t)$, as opposed to the single term $\Phi_i(t_0+\Delta t)$ in the piecewise-constant case. In Appendix A we show the non-linear system of equations (analogous to Eq. (13)) that are used in solving the energy-balance equation using this tilt prescription.

5 Interpolation

In regions where material state properties (*e.g.* opacity, specific heat, etc.) of the slab are smooth and continuous, it is natural to expect that the material temperature (and the sources constructed from the material temperature) is continuous as well. By definition, a piecewise-constant implementation of the temperature can never have sources that are continuous. The tilting prescription for Φ described in the previous section attempts to build sources from temperature profiles that are, loosely speaking, closer to being continuous since the temperature within each zone has been tilted. Perfect continuity is

not achieved because the tilting prescription allows for unequal temperatures at the left and right sides of each zone boundary. This is evident from the fact that interior delta function sources still exist in this prescription for source tilting (*i.e.* Eq. (30)).

In this section we construct a prescription for $\widetilde{\Phi}(x)$ that enforces continuity by linearly interpolating between the Φ_i at the zone centers as depicted in Fig. B.2. Thus the sources are constructed using "shifted" or "offset" zones that have zone edges located at the centers of the original N zones defined in the piecewise-constant discretization. There are $N+1$ such shifted zones, $N-1$ of them being interior, with zone edges being derived from the zone centers of the piecewise-constant discretization, and two half zones on the left and right hand sides of the problem (or adjoining any locations in the problem where the material properties undergo significant change). Because the sources terms are defined on these shifted zones, the Monte Carlo particles are emitted from the shifted zones as well. The energy deposition of the Monte Carlo particles is done in the original zone structure.

In the piecewise-constant discretization, the problem volume is divided into N zones, enumerated by $i \in (1, N)$, with the left edge of zone i being located at x_i and the right edge being located at x_{i+1}. The left edge of an interior *shifted* zone $j \in (2, N-1)$ is $(x_{j-1} + x_j)/2$ and the right edge is $(x_j + x_{j+1})/2$. The interpolated field for interior shifted zone j is given by

$$\widetilde{\Phi}_j(x) = \Phi_{j-1}\left[\frac{x_{j+1} + x_j - 2x}{x_{j+1} - x_{j-1}}\right] + \Phi_j\left[\frac{2x - x_j - x_{j-1}}{x_{j+1} - x_{j-1}}\right] \quad , \tag{32}$$

while the interpolated field for the half zones at the problem boundaries (or equivalently, zone interfaces between significant changes in material properties) are given by

$$\widetilde{\Phi}_1(x) = \widetilde{\Phi}_2(x) \quad , \tag{33}$$

and

$$\widetilde{\Phi}_{N+1}(x) = \widetilde{\Phi}_N(x) \quad . \tag{34}$$

We construct our sources using the interpolated field defined by Eq. (32), and the special cases for the half zones at boundaries.

In the case of source tilting described in Sect. 4 we had the advantage that the scheme for producing the tilted field, $\widetilde{\Phi}_i(x)$, from the piecewise-constant field, Φ_i, conserved the total energy (in the field Φ) within the zone. As a result of this, the $\partial\Phi/\partial t$ source term, when integrated within the zone during the time step, was identical to its piecewise-constant counterpart. This equality is not automatic in the case of interpolation, and as we show below, the integrated time derivative source terms are not identical to their piecewise-constant counterparts in the general case of arbitrary zone sizes.

The gradient sources, on the other hand, do not suffer from this defect. Its source within each interior shifted zone j is given by

$$-\frac{\mu c}{4\pi}\frac{\partial\widetilde{\Phi}_j(x)}{\partial x} = \frac{\mu c}{8\pi}\left[\frac{\Phi_j(t_0+\Delta t)-\Phi_{j-1}(t_0+\Delta t)}{x_{j+1}-x_{j-1}}\right] \quad , \tag{35}$$

remembering that the index j of $\widetilde{\Phi}_j$ refers to the shifted zone j, while the indices on the right hand side of the equation refer to zone indices of the original piecewise-constant discretization. Monte Carlo sampling of this source term is done with a uniform distribution, within the shifted zone, and the unknown factor carried by the particles that must be solved for is $\Phi_j(t_0+\Delta t)-\Phi_{j-1}(t_0+\Delta t)$. Unlike the case for the original piecewise-constant discretization, and the case for source tilting, there are no $\delta(x)$ function sources on the boundaries between zones, except in the case of zone edges adjoining problem boundaries or significant changes in material properties where the continuity is not enforced.

The gradient sources, when integrated over any shifted zone j, are identical to the piecewise-constant integrated sources *within the same region*, since

$$-\mu\int_{\frac{x_j+x_{j+1}}{2}}^{\frac{x_{j+1}+x_{j+2}}{2}} dx\ \frac{\partial B}{\partial x} = -\mu\Delta B = -\frac{\mu c}{4\pi}(\Phi_{j+1}-\Phi_j) \quad . \tag{36}$$

This expression holds if either the interpolated field, Eq. (35), or the piecewise-constant field, Eq. (7), is used. Note that there are no constraints on the sizes of the zones.

In sharp contrast to source tilting, where the interior δ-function sources are only softened, the δ-function sources are completely eliminated when using interpolation, except where sharp discontinuities in the material opacity occur and one would expect a discontinuity in the solution. The strength of the δ-function sources of the original piecewise-constant treatment have now been completely spread across the zones without introducing a new particle type, obtaining the benefit of the improved source treatment without increasing computational overhead.

The time-derivative source within each shifted zone is given by

$$-\frac{1}{4\pi}\frac{\partial\widetilde{\Phi}_j}{\partial t} = -\frac{\delta(t-t_0)}{4\pi}\left[\Delta\Phi_{j-1}\left(\frac{x_{j+1}+x_j-2x}{x_{j+1}-x_{j-1}}\right)+\Delta\Phi_j\left(\frac{2x-x_j-x_{j-1}}{x_{j+1}-x_{j-1}}\right)\right] \quad , \tag{37}$$

where

$$\Delta\Phi_j = \Phi_j(t_0+\Delta t)-\Phi_j(t_0) \quad .$$

Sampling of this source must be done from a linear distribution due to the x-dependence of this term.

We now again integrate this source within the same integration region as was done in Eq. (36), obtaining

$$-\frac{\delta(t-t_0)}{4\pi}\Big(\Delta\Phi_{j+1}[\frac{x_{j+2}-x_{j+1}}{2}]+\Delta\Phi_j[\frac{x_{j+1}-x_j}{2}] \\ -\frac{1}{4}[(x_{j+2}-x_{j+1})-(x_{j+1}-x_j)](\Delta\Phi_{j+1}-\Delta\Phi_j)\Big) \quad . \quad (38)$$

Using only the piecewise-constant time-derivative source, Eq. (8), the analogous integration gives

$$-\frac{\delta(t-t_0)}{4\pi}\left(\Delta\Phi_{j+1}\left(\frac{x_{j+2}-x_{j+1}}{2}\right)+\Delta\Phi_j\left(\frac{x_{j+1}-x_j}{2}\right)\right) \quad . \quad (39)$$

The two expressions above differ by the term $\frac{1}{4}[(x_{j+2}-x_{j+1})-(x_{j+1}-x_j)](\Delta\Phi_{j+1}-\Delta\Phi_j)$, which vanishes if one uses equally spaced zones. For problems that have unequal zone sizes (see Sect. 6.3), we choose to interpolate only the gradient source term, leaving the time derivative term piecewise constant, Eq. (8), thereby preserving energy conservation. This gives satisfactory results.

In Appendix B we show the non-linear system that is constructed when solving the energy balance equation for the case of interpolation.

6 Results

To test the efficacy of our modified source term treatment, we run Marshak wave [12] calculations, comparing our results to the self-consistent piecewise-linear work shown in [5] and to piecewise-constant calculations [11]. We also run some of the benchmark calculations shown in [13], and Larsen's test problem defined in [14]. The latter examples exhibit material opacities that are discontinuous in space as well as being temperature and frequency dependent. Larsen's test problem also requires unequal zone sizes.

6.1 Marshak waves

For these calculations we assume a grey opacity $\sigma = 200/\text{cm}$. Initial conditions consist of a left problem boundary at $x_0 = 0$ in contact with a 1 keV heat bath and an initial temperature of the slab at or near zero. Our heat capacity is .1 jerk/cm-keV (1 jerk = 10^9Joules). To avoid negative excursions of the material temperature (due to the spatial discretization of material properties), we employ a slope limiting procedure similar to that of [15] for our source tilting algorithm. For our interpolation algorithm, we enforce positivity by

replacing any negative temperature excursion at the end of a time step by the initial temperature.

Figure B.4 shows comparisons of a calculated Marshak wave at $t = 30$ shakes (shake=1×10^{-8} seconds) using source tilting and the original piecewise-constant treatment, for: (a) 12.5, (b) 25, (c) 50, and (d) 100 mean free paths (mfp) per zone. The initial temperature of the slab was zero. In each of the four panels of the figure, the top line represents the piecewise-constant calculation, while the bottom line is calculated using the source tilting procedure. As the optical thickness of the zones is decreased, the temperature profile of the Marshak wave changes. The changes are quite significant for the piecewise-constant calculations, and less so for the calculations employing source tilting.

Figure B.5 is completely analogous to Fig. B.4, except that calculations are now performed using our interpolation procedure. Aside from discretization effects near the foot of the Marshak wave, the profiles of the waves when calculated using interpolation are nearly stationary as we vary the zone size. This is especially evident when the results are overlaid, as shown in Fig. B.6 (a). Here we have drawn lines connecting the zone centers for convenience when comparing to the analogous 80 zone (12.5 mfp/zone) result calculated using the self-consistent piecewise-linear method of [5], shown in panel (b). Our results agree very well.

It is clear from our results that source tilting/interpolation improves our Marshak wave calculations by reducing the dependence of propagation speeds on zone sizes. Interpolation of the sources gives propagation speeds with the least sensitivity to zone sizes, even to the point where each zone can contain 100 mfp. Excessive energy flow, in this case, is almost eliminated. This is a remarkable result. In fact, the reason for excessive energy flow in thick systems is clear. In the piecewise-constant treatment all gradient sources (δ-function sources) reside on zone boundaries and directly contribute to energy flow between zones. This is an unphysical effect. In both interpolated and self-consistent piecewise-linear calculations, only those sources born close enough to zone edges contribute to transport. In the case of source tilting, only part of the δ-function sources are spread into the zones. Hence a calculation using source tilting can still suffer from excessive energy flow, though less so than in a piecewise-constant treatment. With the difference formulation, the mechanisms causing unphysical energy flow are easily understood, and remedied.

6.2 Test cases from Reference [13]

The first of two examples from [13] involve using a temperature-dependent opacity of the form $\sigma = \sigma_o/T^3$, where $\sigma_o = 300\,\mathrm{keV}^3/\mathrm{cm}$. The heat capacity

of the slab is .3 jerk/cm-keV. A 1 keV heat bath is in contact with the left side of a slab of width .05 cm. We have performed these calculations using interpolation. Figure B.7 shows results comparing calculations with 10, 20, 50, and 100 zones. Figure B.8 shows similar results, but this time with different time steps of Δt =1.25×10^{-6}, 1.25×10^{-5}, and 1.25×10^{-4} shakes. Our results are stationary as the zone size and time step size are varied. They also agree well with [13] (see Figs. 1, 3, and 4 of [13]).

The second example uses a slab of width .075 cm. The heat capacity is the same as the first example, and the opacity of the slab has a similar $1/T^3$ dependence, where

$$\sigma_o(x) = \begin{cases} 300 \text{ keV}^3/\text{cm} & 0<x<.025 \\ .003 \text{ keV}^3/\text{cm} & .025<x<.05 \\ 300 \text{ keV}^3/\text{cm} & .05<x<.075 \end{cases} .$$

Thus there are significant discontinuities in the material opacity. Within each of the three regions separated by the changes in opacity there are 50 zones (150 zones in the problem). Figure B.9 shows results at various times using interpolation, with continuity enforced across the changes in opacity (red) and discontinuity allowed at the changes in opacity (black). Failing to properly support the physical discontinuity in the solution where the material opacity has a discontinuity produces an error, seen in the kinks in the solution near these changes in opacity. Figure B.10 shows a close-up of Fig. B.9 (c) where the kinks are more readily distinguishable. In panel (d) of Fig. B.9, we show our solution near steady state. This figure differs from the result shown in [13]. However, we believe our solution near steady state to be correct. One would expect the temperature to be (nearly) continuous, allowing only discontinuities in the first derivative at the discontinuities in opacity. One would also expect a monotonically decreasing (going to the right of the slab) solution at steady state. Our result more closely matches these conditions. We suspect that the result shown in [13] has not reached steady state.

The kinks in the solution shown in Fig. B.9 are easily understood. In the difference formulation, any discontinuity in temperature manifests itself as a δ-function source due to the gradient terms in Eq. (5). Temperature discontinuities are present at problem boundaries and where there is significant change in material opacity. By requiring temperature continuity across these changes in opacity, the δ-function source is replaced by a uniform source within the shifted zone that contains the discontinuity. The latter source will produce weaker energy flow across the zone boundary than the original (and physical) δ-function source. Thus there will be insufficient heating and cooling of the zones adjacent to the discontinuities in opacity, causing the kinks seen in Fig. B.9.

6.3 Larsen's test problem

Larsen's test problem is originally defined in [14]. A slab with a thickness of 4 cm is heated by a 1 keV radiative source at the *right* boundary. The heat capacity of the slab is constant, .05109 Jks/cm^3-keV. The opacity is defined as

$$\sigma(\nu, T, x) = \sigma_o(x) \frac{1 - e^{-h\nu/kT}}{(h\nu/keV)^3} \quad ,$$

where

$$\sigma_o(x) = \begin{cases} 1 \text{ keV}^3/\text{cm} & 0<x<1 \\ 1000 \text{ keV}^3/\text{cm} & 1<x<2 \\ 1 \text{ keV}^3/\text{cm} & 2<x<4 \end{cases} \quad .$$

This opacity closely models inverse Bremsstrahlung absorption corrected for stimulated emission. The spatial zoning is also defined as

$$\Delta x = \begin{cases} .10 \text{ cm} & 0<x<1 \\ .02 \text{ cm} & 1<x<2 \\ .20 \text{ cm} & 2<x<4 \end{cases} \quad .$$

As there is no analytic solution, we compare our result with a similar calculation done using a much finer spatial zoning and smaller time step, as seen in Fig. B.11. The plots show results at a time $t = .090$ shakes, or 900 ps, using a time step of .01 shakes (10 ps). We also compare to calculations using the piecewise-constant algorithm (no source tilting) in Fig. B.12. Panel (a) of this figure shows a close-up of the interior optically thick region with calculations using interpolation and zone refinements of 1×, 2×, 4×, and 8× the original zoning. Panel (b) shows the analogous results using the piecewise-constant algorithm. Note the teleportation effects in this latter case, and the slower convergence with zone size refinement. Since this test problem uses unequal zone sizes, we have used piecewise constant $\partial B/\partial t$ sources so as to maintain energy conservation as described previously in Sect. 5. We note that sampling of the frequency in these calculations was simple due to the fact that in the difference formulation, there is no σB source term as in standard formulation calculations. In other words, there was no need for binning the frequency or angular variables. Our results agree very well with those shown in [16].

7 Error Analysis

In [5], it was shown that in a self-consistent piecewise-linear calculation the temperature of a zone during a Marshak wave calculation is second order

accurate. In Fig. B.13 we show similar calculations using our source tilting and interpolation algorithms as well as the original piecewise-constant treatment. The different panels of this figure represent calculations with different gray opacities. All temperatures were taken from the zone residing at 1 cm, after a finite amount of time, as labeled in the plots. We plot the temperatures as a function of photon mean free path/zone, or $\sigma\ \Delta x$, where Δx is the zone width. For small $\sigma\ \Delta x$, the error in the temperature is linear for the source tilting, interpolated, and piecewise-constant calculations, as is evident in the top left panel. This is in stark contrast to the quadratic behavior of the self-consistent piecewise-linear calculations in [5], and is indicative of the accuracy of these discretization schemes in the optically thin limit. Thus, for problems where the zones are optically thin, source tilting and interpolation give no improvement over piecewise-constant calculations, as expected. The situation is different when the zone widths contain many photon mean free paths. For piecewise-constant calculations, teleportation effects (as described in Sect. 3) become pronounced, causing excessive energy flow. This is clearly seen in the panels of Fig. B.13 where $\sigma\ \Delta x > 1$. The source tilting algorithm shows similar behavior, though not as pronounced. Interpolation is the most stationary in this limit, showing very little, if any, energy teleportation. Hence, in the limit of many mean free paths per zone, source tilting, and to an even greater degree interpolation, performs much better than piecewise-constant calculations.

8 Monotonicity issues

Brooks *et al.* [5] showed that a self-consistent piecewise-linear treatment of the material state variable can violate monotonicity for optically thick problems with large temperature gradients. Though our interpolation algorithm is an ad-hoc approximation to a self-consistent piecewise-linear treatment, our results that utilize interpolation can suffer from similar monotonicity violations when working in the optically thick regime. This is in direct contrast to piecewise-constant calculations, where monotonicity violations have not been observed in practice. We will show, however, that monotonicity can be easily preserved in the optically thick limit by interpolating only the gradient sources. Empirically, it seems that by not interpolating the time-derivative sources, we can retain desirable monotonicity characteristics and preserve energy conservation, while minimizing computational cost.

To elucidate these statements, we perform an optically thick limit ($\sigma\Delta x \gg 1$) analysis of the first three zones (labeled 1, 2, and 3) of the slab adjacent to the left problem boundary, as shown in Fig. B.14. A thermal bath, Φ_B, heats the slab at the problem boundary located at position x_1. Within each zone, the field $\Phi(x) = aT^4(x)$ takes on the values Φ_1, Φ_2, and so forth. Panel (a) shows the initial configuration of the system at time t_0. Here all values of Φ_i

are equal to some initial $\Phi_0 \ll \Phi_B$. Panel (b) shows the system after one time step Δt. Here $\Phi_1(t_0+\Delta t) > \Phi_2(t_0+\Delta t) > \Phi_3(t_0+\Delta t)$, and monotonicity is preserved. Panel (c) shows a scenario, where after one time step Δt, we have $\Phi_1(t_0+\Delta t) > \Phi_2(t_0+\Delta t) < \Phi_3(t_0+\Delta t)$, which violates monotonicity. To understand how the scenarios in panel (b) and (c) might occur, it is necessary to look at the net energy flow into zone 2 during the first time step.

8.0.1 Piecewise-constant calculation

In a piecewise-constant calculation, the net energy flow into zone 2 due to gradient sources occurs due to the source located at x_2, from the portion directed in the positive μ direction. Using Eq. (7), the total energy within time Δt is

$$\begin{aligned} -\int_0^{\Delta t} dt \int_0^1 d\mu \, \frac{\mu c}{4\pi}[\Phi_2(t_0+\Delta t) - \Phi_1(t_0+\Delta t)] \\ &= \frac{\Delta t \; c}{8\pi}[\Phi_1(t_0+\Delta t) - \Phi_2(t_0+\Delta t)] \\ &\approx \frac{\Delta t \; c}{8\pi}[\Phi_1(t_0+\Delta t) - \Phi_0] \quad . \end{aligned} \tag{40}$$

In the second line above we have assumed that, due to the large opacity, the change in Φ_2 after one time step (whether it be positive or negative) is small. The expression in Eq. (40) is positive and therefore only contributes to a positive change in Φ_2.

Particles that are born uniformly in zone 1 due to the $\partial B/\partial t$ sources traverse only a short distance before they are re-absorbed due to the large opacity. Thus only particles born near the left side of x_2 traveling in the positive μ direction can traverse into zone 2, thereby contributing to the energy flow into this zone. Consider the source born in an infinitesimal region dx a distance x to the left of x_2, traveling in the positive μ direction. Using Eq. (8), the contribution of sources born in this region that deposit energy in zone 2 within time dt is given by

$$\begin{aligned} d\mu \; dt \; dx \; e^{-\sigma x/\mu} \delta(t-t_0) \frac{-1}{4\pi}[\Phi_1(t_0+\Delta t) - \Phi_1(t_0)] = \\ d\mu \; dt \; dx \; e^{-\sigma x/\mu} \delta(t-t_0) \frac{-1}{4\pi}[\Phi_1(t_0+\Delta t) - \Phi_0] \; . \end{aligned} \tag{41}$$

Integrating over positive μ, x, the time-step interval $[t_0, t_0+\Delta t]$, and extracting the leading order term in $1/\sigma$ gives

$$-\frac{1}{8\pi\sigma}[\Phi_1(t_0+\Delta t) - \Phi_0] \; . \tag{42}$$

Equations (40) and (42) combine to give the net energy flow into zone 2:

$$\left(\frac{\Delta t\ c}{8\pi} - \frac{1}{8\pi\sigma}\right)[\Phi_1(t_0+\Delta t) - \Phi_0]\ . \tag{43}$$

Thus the condition to have positive energy flow into zone 2, and thus respect monotonicity, is $\Delta t\ c > 1/\sigma$, which is easily fulfilled.

8.0.2 Interpolation of the gradient sources

In the case where we interpolate the gradient sources only, the energy flow into zone 2 due to the $\partial B/\partial t$ sources are again given by Eq. (42) (they are identical to piecewise-constant case). The gradient sources, on the other hand, must be calculated using shifted zones. The shifted zone that encompasses half of zone 1 and zone 2, for example, will emit particles uniformly within this region. Thus there will be a significant fraction of particles emitted from this shifted zone that could contribute to zone 2. However, because of the μ dependence of these sources (see Eq. (35)), particles have equal positive or negative weights, depending on the direction of travel. Thus the overall contribution from positive and negative weight particles will in general cancel, except near the zone edge at x_2. The net energy flow within time dt due to volume dx is given by

$$2d\mu\ dt\ dx\ e^{-\sigma x/\mu}\frac{-\mu c}{4\pi\Delta x}[\Phi_2(t_0+\Delta t) - \Phi_1(t_0+\Delta t)] \approx \\ 2d\mu\ dt\ dx\ e^{-\sigma x/\mu}\frac{\mu c}{4\pi\Delta x}[\Phi_1(t_0+\Delta t) - \Phi_0]\ . \tag{44}$$

Here μ points in the positive direction, x is the distance from x_2, and Δx is the zone size. The factor of two is due to the fact that half the contribution will come from sources born to the left of x_2 that traverse into zone 2, and the other half from sources born to the right of x_2 that traverse into zone 1. The latter contribution has negative weight (due to the μ dependence), and when subtracted, contributes to the overall flow across the interface at x_2. Integrating Eq. (44) within time interval $[t_0, t_0+\Delta t]$, x, and positive μ, and taking the leading order term in $1/\sigma$ gives

$$\frac{\Delta t\ c}{6\pi\sigma\Delta x}[\Phi_1(t_0+\Delta t) - \Phi_0]\ . \tag{45}$$

Using Eqs. (42) and (45), the total energy flow into zone 2 is

$$\left(\frac{\Delta t\ c}{6\pi\sigma\Delta x} - \frac{1}{8\pi\sigma}\right)[\Phi_1(t_0+\Delta t) - \Phi_0]\ . \tag{46}$$

Thus the condition for positivity is $\Delta t\ c > \frac{3}{4}\Delta x$, which is not difficult to satisfy.

8.0.3 *Interpolation of the gradient and $\partial B/\partial t$ sources*

Energy flow due to the interpolated gradient sources is given by Eq. (45). The largest contribution of the interpolated $\partial B/\partial t$ source that is born within the shifted zone, contributing energy to zone 2, occurs in the region bounded by the positions x_2 and $(x_2 + x_3)/2$. This is due to the fact that particles born within this region will immediately become re-absorbed (due to the large opacity). Since there is no μ dependence for this source, all particles have the same sign for their weight (regardless of direction) and thus contribute to the energy deposited into zone 2. The net energy change is

$$\begin{aligned}
&\int_{-1}^{1} d\mu \int_{t_0}^{t_0+\Delta t} dt \int_{x_2}^{\frac{x_2+x_3}{2}} dx \left(\frac{-1}{4\pi} \frac{d\widetilde{\Phi}_2}{dt} \right) \\
&\quad = \frac{-1}{4\pi\Delta x} \int_{x_2}^{\frac{x_2+x_3}{2}} dx[\Delta\Phi_1 \ (x_3 + x_2 - 2x) + \Delta\Phi_2 \ (2x - x_1 - x_2)] \\
&\quad \approx \frac{-1}{4\pi\Delta x} \int_{x_2}^{\frac{x_2+x_3}{2}} dx[\Delta\Phi_1 \ (x_3 + x_2 - 2x)] \\
&\quad = \frac{-\Delta x}{16\pi} [\Phi_1(t_0 + \Delta t) - \Phi_0] \quad . \qquad (47)
\end{aligned}$$

Here $\Delta\Phi_i = \Phi_i(t_0 + \Delta t) - \Phi_i(t_0)$ and we have again assumed that the change in Φ_2 is small. Including the gradient sources, the net energy flow into zone 2 in this case is

$$\left(\frac{\Delta t \ c}{6\pi\sigma\Delta x} - \frac{\Delta x}{16\pi} \right) [\Phi_1(t_0 + \Delta t) - \Phi_0] \quad , \qquad (48)$$

and the condition for positivity is $\Delta t \ c > \frac{3}{8}\sigma(\Delta x)^2$. In the limit of large σ (or large zone sizes) this condition is difficult to satisfy. Monotonicity is easily violated in this case.

9 Conclusions

A computational algorithm for the transport of thermally emitted radiation is accurate in the diffusion limit if it successfully addresses two issues. The first is getting the coupling of the energy in the radiation field to that of the material correct. This was noted by [8] and more formally developed in [9]. The second is getting the correct flux between optically thick zones. Algorithms can successfully deal with one, or the other of these two issues independently. As an example, the IMC [6] algorithm does not produce correct coupling of the radiation to the material due to the effective scattering, but it is less subject to problems with energy teleportation, probably also due to effective scattering. The SIMC algorithm, using a finite element piecewise-constant

discretization of the material state variable, gets the local energy coupling correct, but produces excessive flux between optically thick zones.

Algorithms have been developed for transport that use self-consistent linear finite-element techniques that successfully address both of the above requirements for accurate solutions in the diffusion limit. This has been done for both deterministic and Monte Carlo methods. Self-consistent piecewise-linear treatments are, by their nature, more complicated than piecewise-constant treatments of the material state variable. The primary goal of this investigation has been to learn whether or not an ad-hoc piecewise-linear treatment of the source terms, following the lead of [7], is sufficient to produce accurate solutions in the optically thick limit.

We have investigated two strategies for an ad-hoc piecewise-linear treatment of the source terms in the difference formulation for transport of thermally emitted photons. The first strategy is taken directly from [7], translating it to the case of the difference formulation for transport. It demonstrates an improvement for optically thick situations, and an analysis of it points to getting the proper radiation flux in the diffusion limit being the key to success. The second strategy, a linear interpolation of the material state variable between zone centers, gets the flux between zones in the thick limit correct, and thereby delivers the most accurate results in this limit.

Self-consistent piecewise-linear treatments of the material state variable can suffer from problems with monotonicity. We have shown that our source tilting and interpolation algorithms can be subject to monotonicity violations, as compared to piecewise-constant calculations where these problems do not occur in practice. We analyzed a specific situation, in the thick limit, where monotonicity can be violated and derive conditions that must be satisfied to preserve monotonic behavior of the solution. The required condition, for the case of linear interpolation of only the gradient source between zone centers, is easily satisfied, and this method has been found to produce robust and accurate solutions.

We have compared results of our algorithms with published benchmark calculations, obtaining very good agreement in all cases except one. In this lone exception, we have given arguments for why we believe our result is correct. These comparisons give us confidence that our algorithm produces accurate results and is stable for wide ranges of zone sizes and time steps.

Relaxing the requirement of optically thin zones in order to produce an accurate transport simulation is of fundamental importance. While fine zoning might be possible in one dimensional simulations, it is not practical in two, or three, dimensional problems. By finding that interpolation, alone, is sufficient to produce accurate results in the diffusion limit, we simplify the situation for

these simulations, making them more practical.

A Non-linear system using source tilting

Here we follow closely the derivations shown in [5]. Since we solve for the unknown fields Φ by Newton-Raphson iteration, it is necessary to be able to express the quantities in Eq. (10) in terms of Φ and $\partial/\partial\Phi$. The first term of Eq. (10) that involves the unknown field Φ is

$$-\int_{x_i}^{x_{i+1}} dx E_{mat}(T) = -E_i = -\Delta x_i \frac{\rho c_\nu}{a^{1/4}}\ \Phi_i^{1/4}, \tag{A.1}$$

where Δx_i is present due to the integration over the zone and represents the width of that zone. The partial derivative with respect to Φ is required for the Newton Raphson solution of the non-linear system,

$$\frac{\partial E_i}{\partial \Phi_j} = \frac{\rho c_\nu}{a^{1/4}} \frac{1}{4} \Phi_i^{-3/4} \delta_{ij}.$$

Again, as was mentioned in Sect. 4, the unknown terms Φ are evaluated at the end of the time step.

Analogous terms can be derived for the term of Eq. (10) that involves the argument σD. The contribution of Monte Carlo particles at zone j is given by

$$\begin{aligned}
(\sigma D)_j = N_j & \\
&+ \sum_i (DDT_{\text{uniform}})_j^i\ (\Phi_i(t_0) - \Phi_i(t_0+\Delta t)) \\
&+ \left[\sum_i (DDT_{\text{linear}})_j^i\ \{(\Phi_{i+1}(t_0) - \Phi_{i+1}(t_0+\Delta t)) - (\Phi_{i-1}(t_0) - \Phi_{i-1}(t_0+\Delta t))\}\right] \\
&+ \sum_i (DDX_{\text{delta}})_j^i\ \{\left[\frac{3}{4}\right](\Phi_{i-1}(t_0+\Delta t) - \Phi_i(t_0+\Delta t)) + \left[\frac{1}{4}(\Phi_{i+2}(t_0+\Delta t) - \Phi_{i-1}(t_0+\Delta t))\right]\} \\
&+ \left[\sum_i\ (DDX_{\text{uniform}})_j^i\ (\Phi_{i-1}(t_0+\Delta t) + \Phi_{i+1}(t_0+\Delta t))\right].
\end{aligned} \tag{A.2}$$

Here N_j is the contribution from the census particles from the prior time step, $(DDT_{\text{uniform}})_j^i$ is the contribution to zone j from the time-derivative sources emanating from zone i, $(DDT_{\text{linear}})_j^i$ is the contribution to zone j from the time-derivative sources originating from zone i, $(DDX_{\text{delta}})_j^i$ is the contribution from zone-edge delta function sources, and $(DDX_{\text{uniform}})_j^i$ is the contribution to zone j from the uniform gradient sources emanating from zone i. The fields with arguments of t_0 are explicit, whereas the fields with arguments of $t_0 + \Delta t$ are the implicit fields that must be solved. If one elimi-

nates all terms in square brackets, $\Big[\ \Big]$, from Eq. (A.2) one recovers the original piecewise-constant non-linear system. Note the similarity with Eq. (52) of [5].

Since all terms of Eq. (A.2) are linear in the unknown fields $\Phi(t_0 + \Delta t)$, it is straightforward to construct $\partial(\sigma D)_j/\partial\Phi_i$. We do not show this expression explicitly here.

B Non-linear system using interpolation

Since only the sampling of particles is done in the 'shifted' zones, and the scoring of particles is done in the original zones, the expressions for the E_j and $(\sigma D)^i_j$ are similar to those of the previous section. In fact, E_j is identical to Eq. (A.1). (σD) is given by

$$
\begin{aligned}
(\sigma D)_j = N_j & \\
&+ \sum_i (DDT_{\text{uniform}})^i_j \ (\Phi_i(t_0) - \Phi_i(t_0 + \Delta t)) \\
&+ \sum_i (DDT_{\text{linear}})^i_j \ \{(\Phi_{i+1}(t_0) - \Phi_{i+1}(t_0 + \Delta t)) - (\Phi_{i-1}(t_0) - \Phi_{i-1}(t_0 + \Delta t))\} \\
&+ \sum_i \ (DDX_{\text{uniform}})^i_j \ (\Phi_{i-1}(t_0 + \Delta t) + \Phi_{i+1}(t_0 + \Delta t)).
\end{aligned}
\tag{B.1}
$$

The definitions of the various terms have been given in the previous section. Note that there are no delta function contributions, since in these terms vanish when using the interpolation scheme. The index j runs through the original zones (*i.e.* $j = 1, N$), whereas the index i runs through the 'shifted' zones (*i.e.* $i = 1, N + 1$).

If one chooses not to interpolate the time-derivative sources, one simply has

$$
\begin{aligned}
(\sigma D)_j = N_j & \\
&+ \sum_i (DDT_{\text{uniform}})^i_j \ (\Phi_i(t_0) - \Phi_i(t_0 + \Delta t)) \\
&+ \sum_i \ (DDX_{\text{uniform}})^i_j \ (\Phi_{i-1}(t_0 + \Delta t) + \Phi_{i+1}(t_0 + \Delta t)).
\end{aligned}
\tag{B.2}
$$

In this case one retains the original number of particle types as in a piecewise-constant implementation of the difference formulation (but not the same types).

References

[1] E. Larsen, The asymptotic diffusion limit of discretized transport problems, Nucl. Sci. and Eng. 112 (1992) 336–346.

[2] D. Knoll, J. Morel, L. Margolin, M. Shashkov, Physically motivated discretization methods, Los Alamos Science 29 (2005) 188–212.

[3] J. Morel, T. Wareing, K. Smith, A linear-discontinuous spatial differencing scheme for s_n radiative transfer calculations, J. Comp. Phys. 128 (1996) 445–462.

[4] J.-F. Clouet, G. Samba, Asymptotic diffusion limit of the symbolic monte-carlo method for the transport equation, J. Comp. Phys. 195 (2004) 293.

[5] E. Brooks III, A. Szoke, J. Peterson, Piecewise linear descretization of symbolic implicit monte carlo radiation transport in the difference formulation, J. Comp. Phy. (submitted).

[6] J. Fleck, J. Cummings, An implicit monte carlo scheme for calculating time and frequency dependent radiation transport, J. Comp. Phys. 8 (1971) 313.

[7] J. Fleck, E. Canfield, A random walk procedure for improving the computational efficiency of the implicit monte carlo method for nonlinear radiation transport, J. Comp. Phys. 54 (1984) 508–523.

[8] T. N'kaoua, Solution of the nonliinear radiative transfer equations by a fully implicit matrix monte carlo method coupled with the rosseland diffusion equation via domain decomposition, SIAM J. Sci. Stat. Comput. 12 (1991) 505.

[9] J. Densmore, E. Larsen, Asymptotic equilibrium diffusion analysis of time-dependent monte carlo methods for grey radiative transfer, J. Comp. Phys. (in press).

[10] A. Szoke, E. Brooks III, The transport equation in optically thick media, J. Quant. Spect. Rad. Tran. 91 (2005) 95.

[11] E. Brooks III, M. McKinley, F. Daffin, A. Szoke, Symbolic implicit monte carlo radiation transport in the difference formulation: a piecewise constant descretization, J. Comp. Phys. 205 (2005) 737–754.

[12] R. Marshak, Note on the spherical harmonic method as applied to the milne problem for a sphere, Phys. Rev. 71 (1947) 443–446.

[13] J. Morel, B. Adams, T. Noh, J. McGhee, T. Evans, T. Urbatsch, Spatial discretizations for self-adjoint forms of the radiative transfer equations, J. Comp. Phys. 214 (2006) 12.

[14] E. Larsen, A grey transport acceleration method for time-dependent radiative transfer problems, J. Comp. Phys. 78 (1987) 459.

[15] B. Cockburn, Devising discontinuous galerkin methods for non-linear hyperbolic conservation laws, J. Comp. App. Phys. 128.

[16] B. Chang, The incorporation of the semi-implicit linear equations into newton's method for solving radiative transfer equations, J. Comp. Phys. (in press).

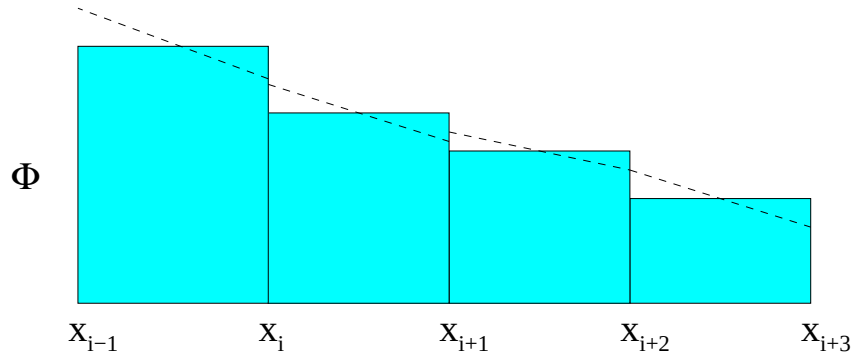

Fig. B.1. (Color online) Example of source tilting (dashed lines) constructed from a piecewise-constant $\Phi = aT^4$ profile (shaded regions).

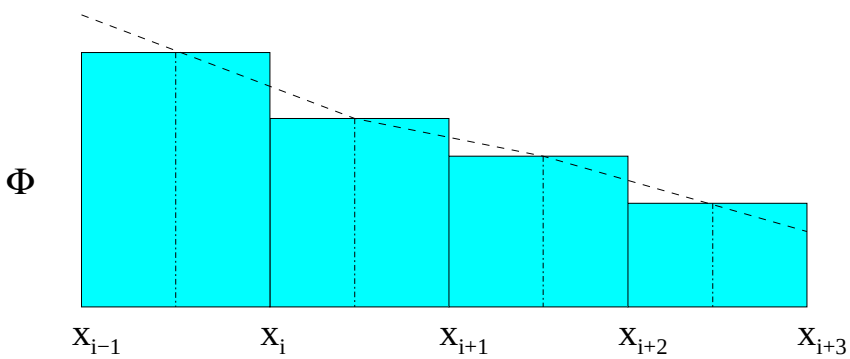

Fig. B.2. Example of interpolation (dashed lines) constructed from a piecewise-constant $\Phi = aT^4$ profile (shaded regions). The dot-dashed lines indicate the zone boundaries of the 'shifted' zones used for source sampling, as explained in the text.

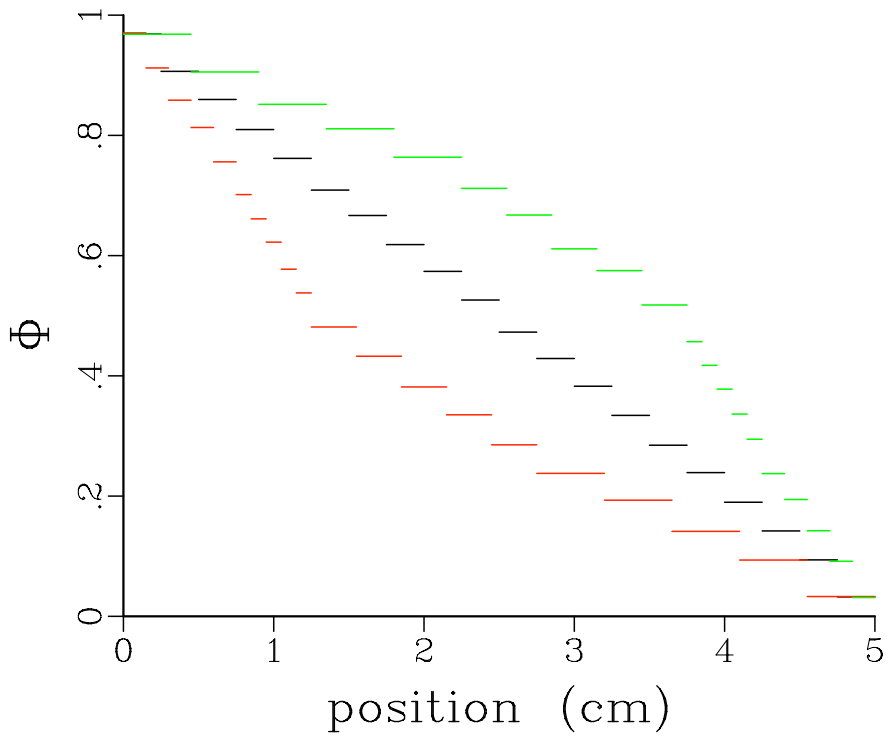

Fig. B.3. Examples of steady-state solutions of $\Phi(x) = aT^4(x)$ using the piece-wise-constant algorithm in the thick limit with constant opacity. All calculations had the same initial conditions, the only difference being the zone sizes (see text).

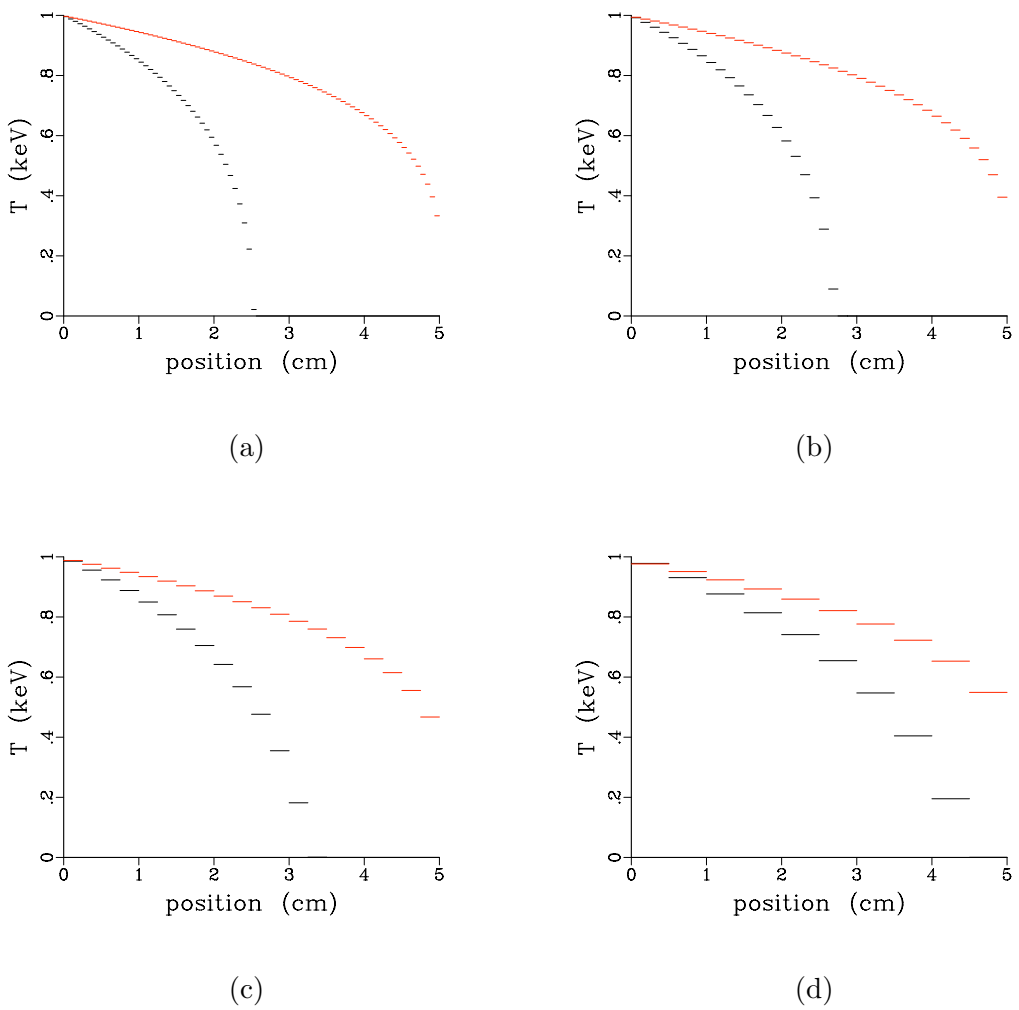

Fig. B.4. Comparison of tilting versus the original piecewise-constant treatment for a 1keV driven Marshak wave at $t = 30$ shakes with initial slab temperature being zero. Panel (a) represents a calculation using 12.5 mfp/zone, (b) 25 mfp/zone, (c) 50 mfp/zone, and (d) 100 mfp/zone. In each panel, the top (red) curve is the piecewise-constant result, while the bottom (black) curve is the result using tilting.

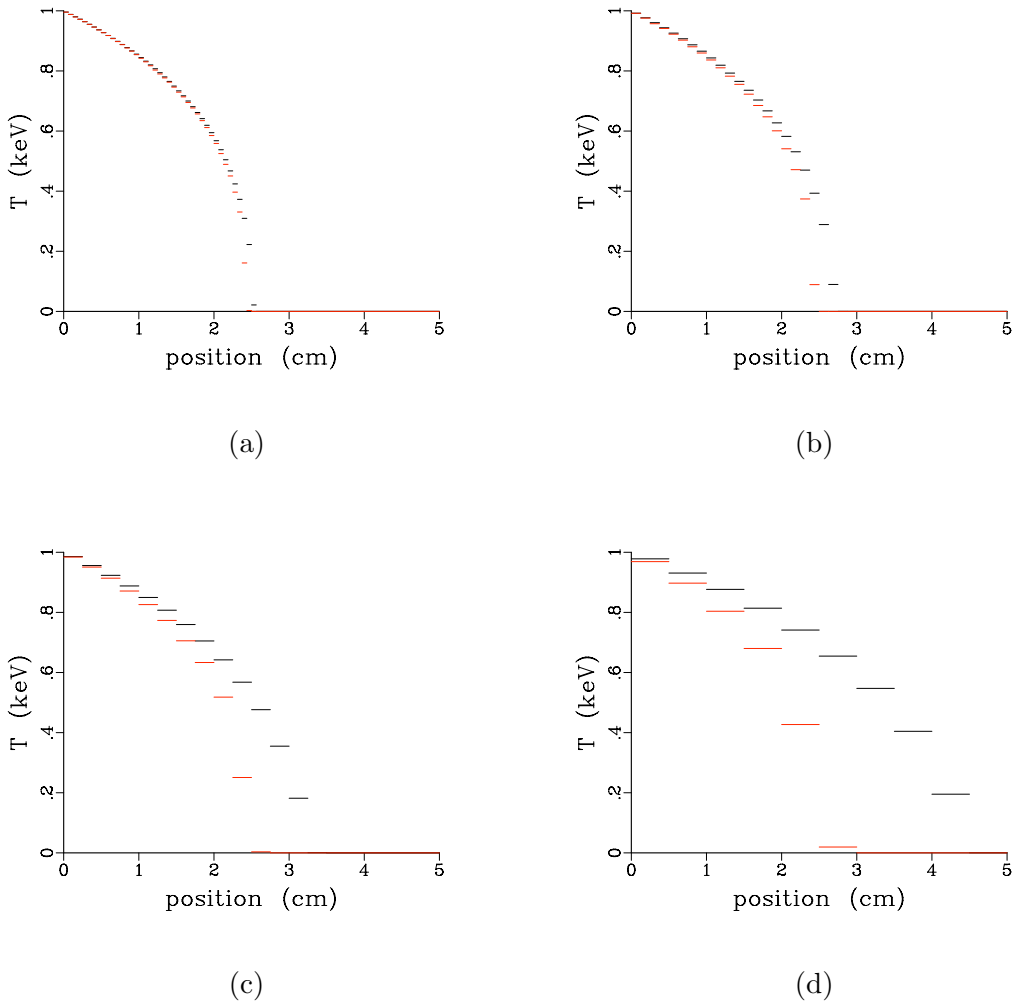

Fig. B.5. Comparison of interpolation versus tilting treatment for a 1keV driven Marshak wave at $t = 30$ shakes with initial slab temperature being zero. Panel (a) represents a calculation using 12.5 mfp/zone, (b) 25 mfp/zone, (c) 50 mfp/zone, and (d) 100 mfp/zone. In each panel, the top (black) curve is the tilting result, while the bottom (red) curve is the result using interpolation.

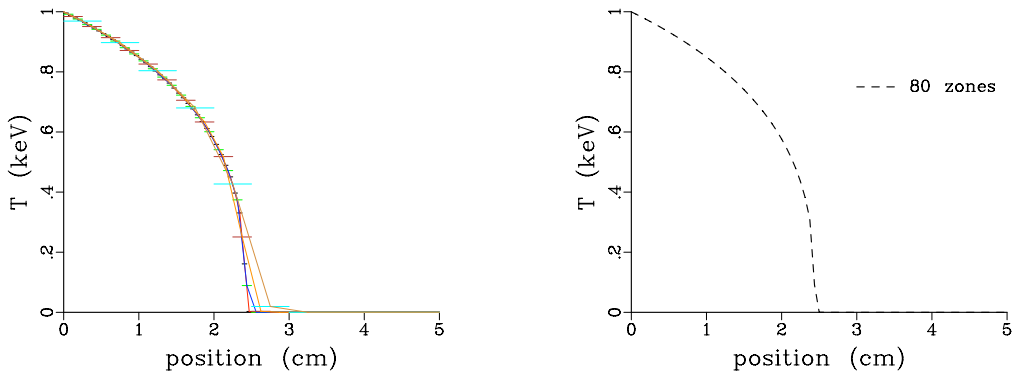

(a) (b)

Fig. B.6. Panel (a) shows overlay of calculations using interpolation for 12.5, 25, 50, and 100 mfp/zone (shown in Fig. B.5) at $t = 30$ shakes. Lines have been connected between centers of zones to facilitate comparison with panel (b), which shows an analogous 80 zone (12.5 mfp/zone) self-consistent piecewise-linear calculation developed by Brooks *et al.* [5].

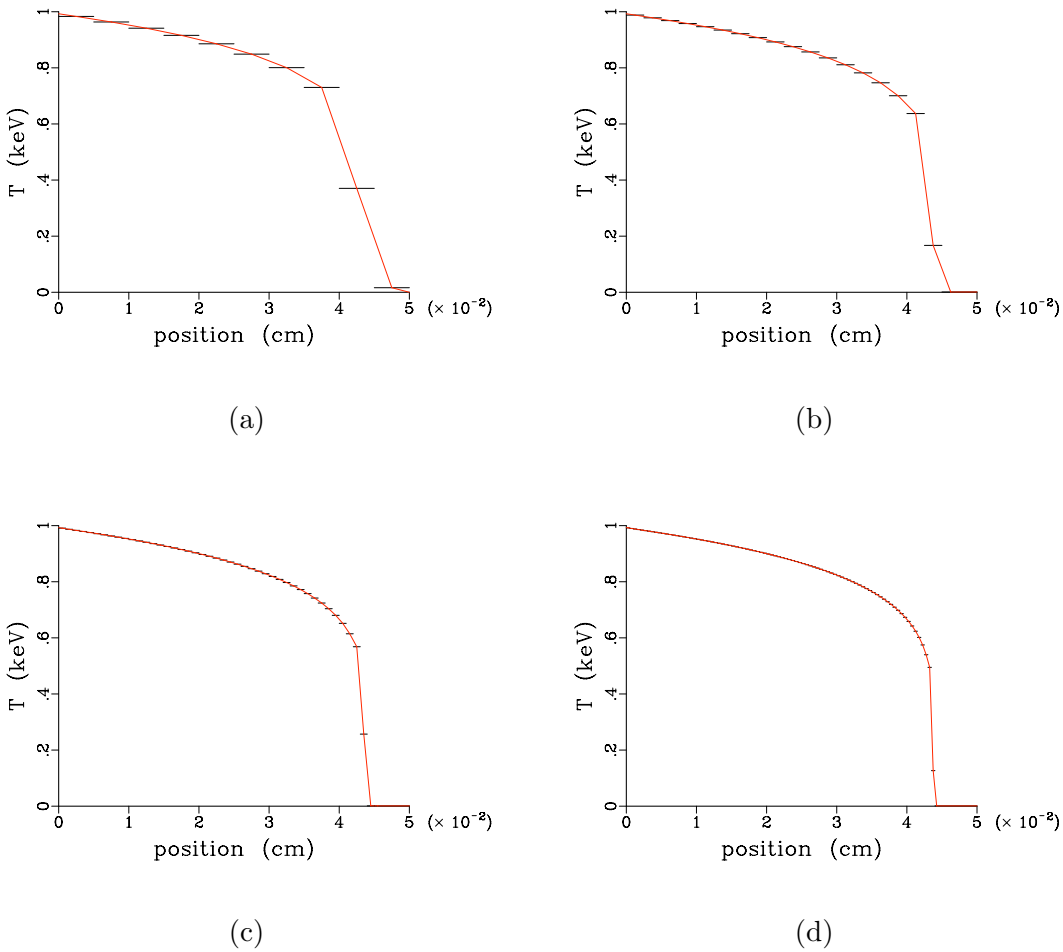

Fig. B.7. Results of the first test example taken from [13] after total time $t = .1$ shakes. Panel (a) shows results for 10 total zones, (b) for 20 total zones, (c) for 50 total zones, and (d) for 100 total zones. We have connected lines between the center of each zone so as to help facilitate comparison with results shown in [13].

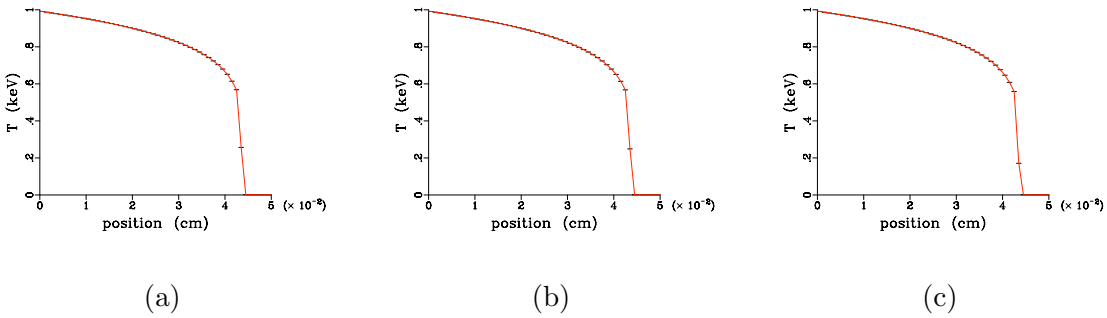

Fig. B.8. Results of the first test example taken from [13] at time $t = .1$ shakes but using different time step sizes Δt. Panel (a) shows results using Δt=1.25×10^{-6}, (b) Δt=1.25×10^{-5}, and (c) Δt=1.25×10^{-4}. All of these calculations used 50 zones.

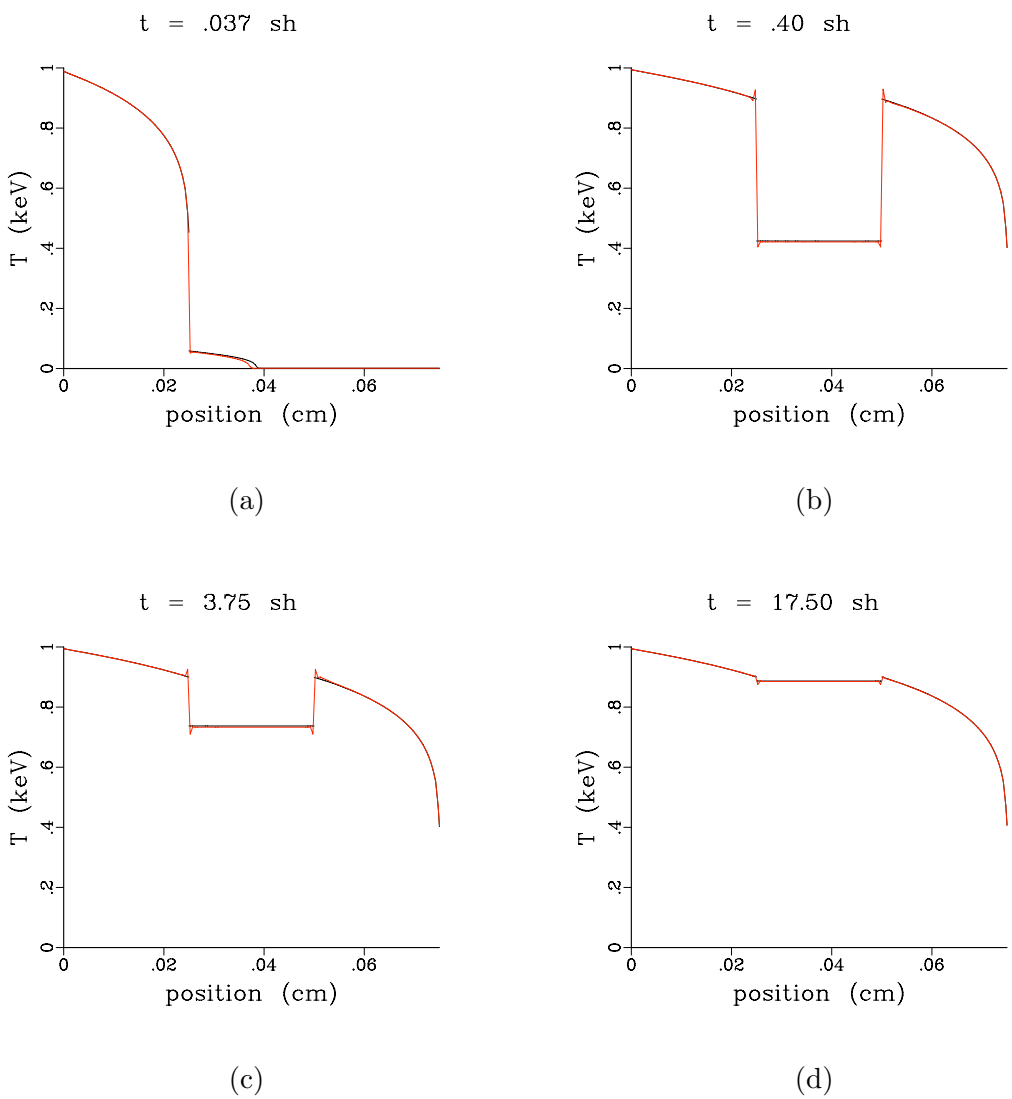

Fig. B.9. Results of the second test example taken from [13] at different times (in shakes) as shown in the plots. The black lines are calculations where discontinuities are supported at zone interfaces where opacity changes occur. The red lines are calculations where discontinuities are supported only at the problem boundaries on each side of the slab. Note the kinks around the positions where the opacity changes in this case. Figure B.10 shows a close up of panel (c).

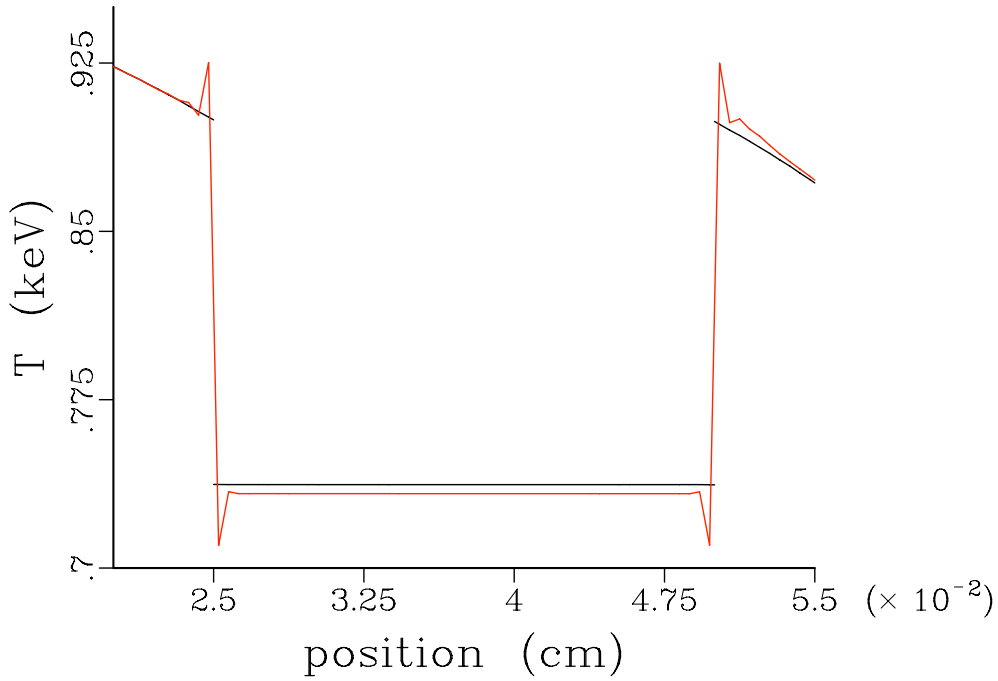

Fig. B.10. Close up of Fig. B.9c, showing the region near the discontinuities in opacity.

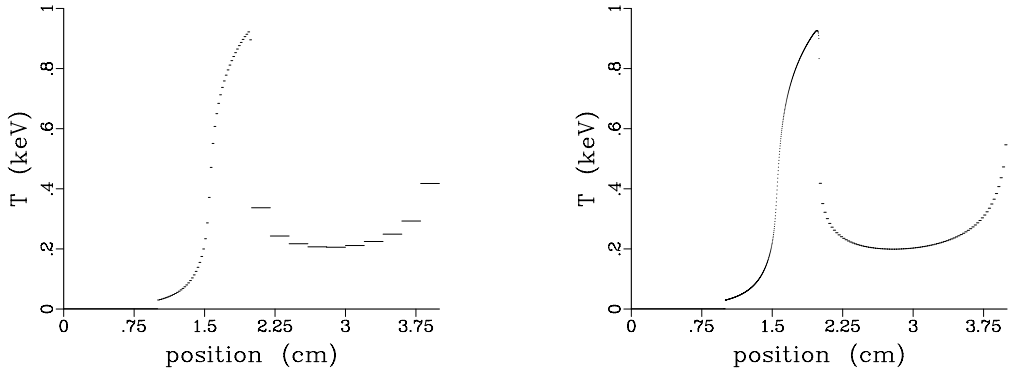

(a) (b)

Fig. B.11. Plot (a) shows the result of Larsen's test problem at total time $t = .09$ shake using Δt=.001 shake and spatial zoning as defined in the text. Plot (b) shows the same calculation but with a zoning that is eight times smaller.

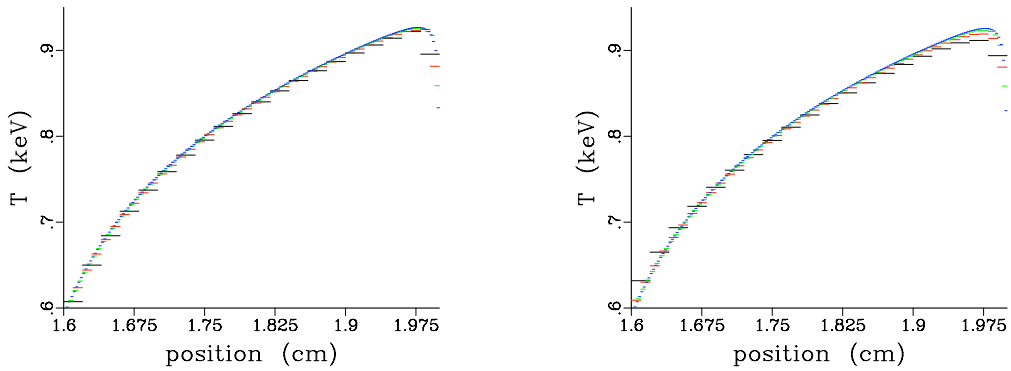

(a) (b)

Fig. B.12. Plot (a) shows a close up of Larsen's test problem at $t = .09$ shake using our interpolation algorithm with 1×, 2×, 4×, and 8× the original zoning. Plot (b) shows similar results, but without source tilting. Note the effects of teleportation and the stronger dependence on zone sizes in the latter case.

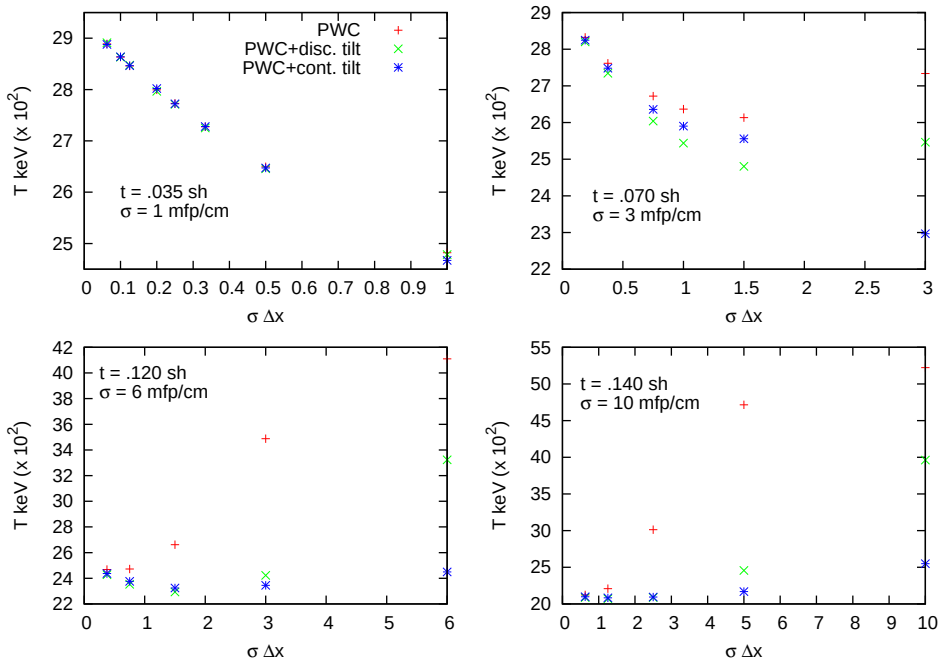

Fig. B.13. Temperature of zone at 1 cm after a finite time during Marshak wave calculations. Each panel shows results for different material opacities and different times, as labeled. The x axis is plotted in units of mean free paths per zone. Δx represents the zone size.

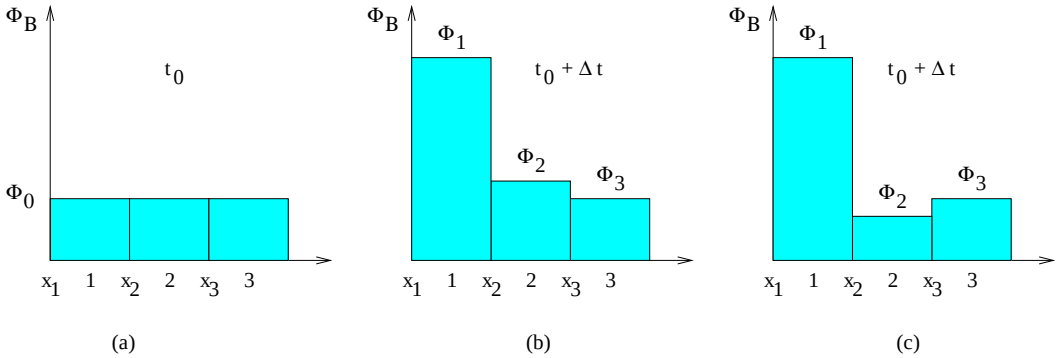

Fig. B.14. Figure depicting scenario used for thick limit analysis in Sect. 8. Panel (a) shows the initial conditions at time t_0. Panel (b) shows a scenario after one time step Δt where the values of the field $\Phi(x)$ preserve monotonicity. Panel (c) shows a scenario after one time step where monotonicity is not preserved.